A comparison between two solution techniques to solve the equations of linear isostasy

Erik Bängtsson *and Björn Lund †

Abstract

In this paper we compare two models to compute the isostatic response of the Earths lithosphere to an external load. The lithosphere is modeled as a linear elastic solid. The two models differ in the mathematical formulation of the problem, their applicability in the incompressible limit, the choice of the finite elements used for discretization, and the solution strategy for the arising algebraic problem. The efficiency and accuracy of both models are compared via extensive numerical experiments in 2D and 3D.

Keywords: glacial isostatic adjustment, FEM, ABAQUS, saddle point matrices, direct vs. iterative solution methods

1 Introduction

In many fields of science, due to practical, technical, and/or economical obstacles, it is not possible to perform classical experiments to obtain answers to many important questions. In geophysics, for example, where time and length scales can be enormous, there are problems which cannot be tackled by laboratory or field experiments due to their sheer size.

One particular problem from the latter field which has attracted much attention lately is the simulation of the response of the outer part of the Earth, the lithosphere, to glacial advance and retreat. The study of glacial isostatic adjustment (GIA) has a long history, first as an explanation to the land uplift observed particularly in Scandinavia and then as a means to estimate the viscosity of the Earth's interior. Lately, GIA studies have become increasingly important for long term safety predictions of nuclear waste repositories at northerly latitudes and for predictions of ice retreat and sea-level increase due to global warming. Since ice sheet growth and thinning over wast areas is impossible to simulate in a laboratory, modeling and computer simulations are our only means to approach the problem.

Techniques and methods for the modeling of GIA has developed rapidly during the last decade. Traditionally based on spectral decomposition in relaxation modes e.g. [19, 22, 20], the current move to incorporate lateral variations in the Earth's composition, its spherical shape and gravitation has lead to the adaptation of various finite element techniques e.g.

*Department of Information Technology, Uppsala University, Box 337, SE-751 05 Uppsala, Sweden, Erik.Bangtsson@it.uu.se

†Department of Earth Sciences, Uppsala University, Villavägen 16, SE-752 36 Uppsala, Sweden, Bjorn.Lund@geo.uu.se

[15, 23, 21, 14]. Other efforts have been directed at incorporating the effects of changing sea-levels and the rotation of the Earth, e.g. [12, 17, 18] and investigations into the effects of compressibility on GIA predictions e.g. [11, 13].

The aim of this paper is to compare the accuracy and efficiency of two approaches to discretize the equations of linear isostasy for GIA, and to solve the arising linear system of equations. Here we will limit ourselves to the elastic problem and not include viscoelasticity. Although this is seemingly a serious limitation in GIA, the result of the study will never the less be of importance on shorter time scales when the glacial load is rapidly changing, if combined with viscoelastic models. Furthermore, when doing numerical simulation of a viscoelastic solid, the need to compute the purely elastic response of the material to a given load arises in each time step. As the geological time-scale that is considered is huge (100 000 yrs), it is of paramount importance for the overall accuracy and efficiency of the viscoelastic solver that the numerical solution method for the elastic problem is accurate and fast. Below we will refer to the two different approaches as Framework I and II.

The first framework considered here is a reformulation of the equations of linear isostasy into a form that is easily implemented in standard finite element (FE) packages, as developed e.g. by [21] and references therein. A major restriction when using general purpose commercial FE packages is that they are not designed to handle even the simplest form of the momentum equation for the GIA problem.

The second framework considered in the paper is a more complete description of the GIA problem and a reformulation of the equations into a mixed variables form. The benefits of Framework II are two-fold. First, we are able to solve a much more detailed momentum equation for GIA, excluding only the gravitational term, and second, the mixed variables form allows us to treat also purely incompressible solids. In this second framework we solve the arising algebraic linear system, which has a matrix of saddle-point form, by a numerically efficient preconditioned iterative solution method. This is in contrast and compared with the highly optimized direct solution method used in the general commercial FE package. For Framework II we have developed our own code based on established open-source finite element and numerical linear algebra (NLA) packages.

In this paper we show that (1) the accuracy of the solution from Framework II is higher than the accuracy of the solution from Framework I, and (2) the preconditioned iterative solution method is more efficient with respect to solution time compared to the direct solver used in the commercial FE package. The higher quality of the solution from Framework II is due to the advection terms actually being included in the model, and not added to the problem as boundary conditions.

This paper is organized as follows. Section 2 contains a general description of the target problem, and in Section 3 and Section 4 the two solution frameworks are described. Section 5 contains results from numerical experiments, and some conclusions are drawn in Section 6.

2 Problem description

The target boundary value problem (BVP) we consider is the incremental momentum equation for quasi-static perturbations of a homogeneous, (visco)elastic continuum in a constant gravity field,

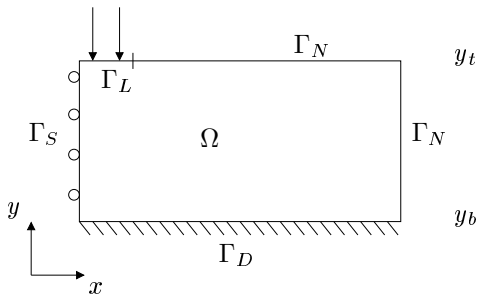

Figure 1: The geometry of the problem

$$-\nabla \cdot \sigma - \nabla(\mathbf{u} \cdot \nabla p_0) + (\nabla \cdot \mathbf{u})\nabla p_0 = \mathbf{f} \text{ in } \Omega \subset \mathbb{R}^d,\ d = 2, 3, \tag{1a}$$

with boundary conditions

$$\sigma(\mathbf{u}) \cdot \mathbf{n} = \ell \text{ on } \Gamma_L \tag{1b}$$
$$\sigma(\mathbf{u}) \cdot \mathbf{n} = \mathbf{0} \text{ on } \Gamma_N \tag{1c}$$
$$\mathbf{u} = \mathbf{0} \text{ on } \Gamma_D \tag{1d}$$

The geometry of the problem is shown in Figure 1 (the domain is symmetric with respect to Γ_S).

In Equation (1), σ denotes the Cauchy stress tensor, $\mathbf{u} = [u_i]_{i=1}^d$ are the displacements, p_0 is the so-called *pre-stress*, $\mathbf{f}$ is a body force, and ℓ is a surface load. The third term on the left hand side of Equation (1a) describes the *buoyancy* of the compressed material, and it vanishes for purely incompressible material since $\nabla \cdot \mathbf{u} = 0$. The second term describes the advection of the pre-stress, which is a hydrostatic stress that is present in the solid before the application of any external load. The hydrostatic pre-stress is given by

$$p_0 = \rho_r g(y_t - y), \tag{2}$$

where g is the gravitational acceleration, ρ_r is the density of the material and y_t is a reference surface (e.g. the Earth's surface). From Equation (2) it follows that

$$\nabla p_0 = -\rho_r g \hat{\mathbf{y}},$$

where $\hat{\mathbf{y}}$ is the unit vector in positive y-direction. For further details on the model and the origin of Equation (1a) we refer, for example, to [21].

Equation (1a) differs from the standard moment balance equation for elastic solids

$$-\nabla \cdot \sigma(\mathbf{u}) = \mathbf{f}, \tag{3}$$

due to the presence of the first order terms $\nabla(\mathbf{u} \cdot \nabla p_0)$ and $(\nabla \cdot \mathbf{u})\nabla p_0$. In order to bridge the gap between Equation (1a) and Equation (3), we introduce the following two models, $C0$ and $C1$, where one or both of these terms are omitted. That is,

$$\text{C0}: \quad (\nabla \cdot \mathbf{u})\nabla p_0 - \nabla(\mathbf{u} \cdot \nabla p_0) = \mathbf{0}. \tag{4a}$$
$$\text{C1}: \quad (\nabla \cdot \mathbf{u})\nabla p_0 = \mathbf{0}. \tag{4b}$$

At first glance, Model $C1$ is a restriction of Equation (1a) and this is also the case for compressible materials, where model $C1$ ignores the buoyancy

term. In the incompressible limit, however, where $\nabla \cdot \mathbf{u} = 0$, model $C1$ gives a correct description of the problem. In Model $C0$, Equation (1) is reduced to Equation (3). This reduced model is introduced to ease the study of the impact of the pre-stress advection term on model performance in the compressible and incompressible cases.

For a homogeneous, isotropic, linear, and purely elastic lithosphere, the Cauchy stress tensor is given by Hooke's law,

$$\sigma(\mathbf{u}) = 2\mu\varepsilon(\mathbf{u}) + \lambda(\nabla \cdot \mathbf{u})I, \tag{5}$$

where $\varepsilon(\mathbf{u}) = 0.5(\nabla\mathbf{u} + \nabla\mathbf{u}^T)$ is the strain tensor, and I is the identity tensor. The parameters $\mu = E/2/(1+\nu)$, $\lambda = 2\mu\nu/(1-2\nu)$ are the Lamé coefficients, and E and ν are the Young's modulus and the Poisson's ratio, respectively.

Remark 2.1 *The description of the Earth as a purely elastic solid is a simplification, but nevertheless important to study. Efficient solution techniques for the purely elastic problem are of great importance for the simulation of a viscoelastic solid since the response of a viscoelastic solid at a given time t_k is a combination of the instantaneous, purely elastic response, and a memory term, an integral over all the previous responses. The memory term is numerically computed as a sum of weighted Hookean responses at all previous times t_i, $i = 0, \ldots, k-1$, and these responses must be computed efficiently in order to achieve an efficient viscoelastic solver.*

Remark 2.2 *For simplicity the Earth is assumed to be homogeneous with respect to the material parameters λ and μ. This simplification does not violate the generality of the obtained results. The numerical solution methods are straightforwardly applicable for inhomogeneous materials.*

After combining Equation (1a) and Equation (5), we arrive at the equations of linear isostasy, formulated in terms of the displacements $\mathbf{u}$, which is the basic model equation used in this study,

$$-\nabla \cdot (2\mu\varepsilon(\mathbf{u})) - \nabla(\mathbf{u} \cdot \nabla p_0) + (\nabla \cdot \mathbf{u})\nabla p_0 - \lambda\nabla(\nabla \cdot \mathbf{u}) = \mathbf{f}, \tag{6}$$

A finite element discretization of Equation (6) together with the boundary conditions in Equations (1b) through (1d) gives rise to the algebraic problem

$$\mathcal{A}\mathbf{x} = \mathbf{b}, \tag{7}$$

where $\mathcal{A} \in \mathbb{R}^{N_u \times N_u}$ is a large and sparse matrix, and $\mathbf{x} \in \mathbb{R}^{N_u}$ and $\mathbf{b} \in \mathbb{R}^{N_u}$ are vectors.

We consider now two settings (frameworks) to approach the target physical phenomenon. The frameworks are defined below and compared throughout the paper, and they differ in (i) the formulation of Equation (6), (ii) the FE discretization of the partial differential equation (PDE), and (iii) the solution strategy for Equation (7).

3 Framework I: ABAQUS

As the name suggests, the first framework is based on the features included in the commercial finite element package ABAQUS[1]. ABAQUS is a highly optimized package, which uses up-to-date numerical techniques and

fully utilizes crucial computer resources such as cache memory, hardware architecture, and buses.

However, ABAQUS is not primarily designed for geophysical applications and therefore not very suitable to model problems of the type of Equation (1a) or Equation (6). It is better suited to using the standard form of the moment balance equation for an elastic solid, Equation (3), that is, a problem without the first order terms arising from the pre-stress advection and the buoyancy.

A remedy to this problem is the introduction of the modified stress tensor [21]

$$T(\mathbf{u}) = \sigma(\mathbf{u}) + \mathbf{u} \cdot \nabla p_0 I, \tag{8}$$

where I is the identity tensor. Substitution of Equation (8) into Equation (1) gives,

$$-\nabla \cdot T(\mathbf{u}) + (\nabla \cdot \mathbf{u})\nabla p_0 = \mathbf{f} \qquad \text{in } \Omega, \tag{9a}$$

$$T(\mathbf{u}) \cdot \mathbf{n} = \ell + \mathbf{u} \cdot \nabla p_0 \mathbf{n} \qquad \text{on } \Gamma_L \tag{9b}$$

$$T(\mathbf{u}) \cdot \mathbf{n} = \mathbf{u} \cdot \nabla p_0 \mathbf{n} \qquad \text{on } \Gamma_N \tag{9c}$$

$$\mathbf{u} = \mathbf{0} \qquad \text{on } \Gamma_D \tag{9d}$$

$$u_1 = 0, \quad \partial_x u_2 = 0 \qquad \text{on } \Gamma_S, \tag{9e}$$

where the symmetry boundary condition in Equation (9e) is added. Equation (9a) is still not of the same form as Equation (3) due to the buoyancy term $(\nabla \cdot \mathbf{u})\nabla p_0$. Therefore, within the ABAQUS framework, we are limited to treat solids described by Model $C0$ or $C1$, that is, without the first order term due to buoyance and with a choice of neglecting the pre-stress term or not. This is a limitation imposed by the modeling tools provided by ABAQUS in its current design. It can be circumvented, see [21] for details, if the buoyancy term is included by coupling external computations to the analysis in an iterative procedure. This is, however, a cumbersome strategy. Due to this limitation, we omit the buoyancy term in the analysis of the problem throughout this section.

A second limitation is related to how the modified stress tensor $T(\mathbf{u})$ is represented, which we outline below. When Equation (9) is solved in ABAQUS, the tensor $T(\mathbf{u})$ is represented internally by a stress tensor $\sigma(\widetilde{\mathbf{u}})$, which is given by Hooke's law,

$$\sigma(\widetilde{\mathbf{u}}) = 2\mu\varepsilon(\widetilde{\mathbf{u}}) + \lambda(\nabla \cdot \widetilde{\mathbf{u}})I. \tag{10}$$

This is a tensor where the pre-stress advection term in $T(\mathbf{u})$ is not present, and in order to compensate for this the modified displacements $\widetilde{\mathbf{u}}$ are introduced in Equation (10). These displacements are related to $\mathbf{u}$, and they are implicitly defined by the tensor equality

$$\sigma(\widetilde{\mathbf{u}}) = T(\mathbf{u}). \tag{11}$$

For the Model $C0$, $\mathbf{u}$ coincides with $\widetilde{\mathbf{u}}$, but for the Model $C1$, $\mathbf{u}$ is in general not equal to $\widetilde{\mathbf{u}}$.

Combining Equations (9), (10), and (11), the following BVP, expressed

in $\mathbf{u}$ and $\widetilde{\mathbf{u}}$, is achieved,

$$
\begin{aligned}
-\nabla \cdot \sigma(\widetilde{\mathbf{u}}) &= \mathbf{f} && \text{in } \Omega, && (12a)\\
\sigma(\widetilde{\mathbf{u}}) &= T(\mathbf{u}) && \text{in } \Omega && (12b)\\
\sigma(\widetilde{\mathbf{u}}) \cdot \mathbf{n} &= \ell + \mathbf{u} \cdot \nabla p_0 \mathbf{n} && \text{on } \Gamma_L && (12c)\\
\sigma(\widetilde{\mathbf{u}}) \cdot \mathbf{n} &= \mathbf{u} \cdot \nabla p_0 \mathbf{n} && \text{on } \Gamma_N && (12d)\\
\mathbf{u} &= \mathbf{0} && \text{on } \Gamma_D && (12e)\\
u_1 = 0, \quad \partial_x u_2 &= 0 && \text{on } \Gamma_S. && (12f)
\end{aligned}
$$

We can eliminate the displacements variable $\mathbf{u}$ by introduction of the transformation ϕ, which is defined such that

$$\widetilde{\mathbf{u}} = \phi(\mathbf{u}).$$

By introducing ϕ, Equation (12) takes the form

$$
\begin{aligned}
-\nabla \cdot \sigma(\widetilde{\mathbf{u}}) &= \mathbf{f} && \text{in } \Omega, && (13a)\\
\sigma(\widetilde{\mathbf{u}}) \cdot \mathbf{n} &= \ell + \phi^{-1}(\widetilde{\mathbf{u}}) \cdot \nabla p_0 \mathbf{n} && \text{on } \Gamma_L && (13b)\\
\sigma(\widetilde{\mathbf{u}}) \cdot \mathbf{n} &= \phi^{-1}(\widetilde{\mathbf{u}}) \cdot \nabla p_0 \mathbf{n} && \text{on } \Gamma_N && (13c)\\
\phi^{-1}(\widetilde{\mathbf{u}}) &= \mathbf{0} && \text{on } \Gamma_D && (13d)\\
\left[\phi^{-1}(\widetilde{\mathbf{u}})\right]_1 = 0, \quad \partial_x \left[\phi^{-1}(\widetilde{\mathbf{u}})\right]_2 &= 0 && \text{on } \Gamma_S. && (13e)
\end{aligned}
$$

The transformation ϕ is a formal construction and it is difficult (not to say impossible) to construct it in the general case. It is therefore approximated by the identity function, such that $\widetilde{\mathbf{u}} = \mathbf{u}$, see for example [21]. We can see the effects of this first order approximation if we examine and compare the components of $\sigma(\widetilde{\mathbf{u}})$ and $T(\mathbf{u})$ term by term.

Expressed in Cartesian coordinates in two space dimensions, the components of $\sigma(\widetilde{\mathbf{u}})$ are

$$
\begin{aligned}
\sigma(\widetilde{\mathbf{u}})_{11} &= (2\mu + \lambda)\frac{\partial \widetilde{u}_1}{\partial x} + \lambda \frac{\partial \widetilde{u}_2}{\partial y} && (14a)\\
\sigma(\widetilde{\mathbf{u}})_{12} &= \mu \left(\frac{\partial \widetilde{u}_1}{\partial y} + \frac{\partial \widetilde{u}_2}{\partial x} \right) && (14b)\\
\sigma(\widetilde{\mathbf{u}})_{21} &= \mu \left(\frac{\partial \widetilde{u}_1}{\partial y} + \frac{\partial \widetilde{u}_2}{\partial x} \right) && (14c)\\
\sigma(\widetilde{\mathbf{u}})_{22} &= (2\mu + \lambda)\frac{\partial \widetilde{u}_2}{\partial y} + \lambda \frac{\partial \widetilde{u}_1}{\partial x}. && (14d)
\end{aligned}
$$

Similarly, the components of $T(\mathbf{u})$ read,

$$
\begin{aligned}
T(\mathbf{u})_{11} &= (2\mu + \lambda)\frac{\partial u_1}{\partial x} + \lambda \frac{\partial u_2}{\partial y} + u_2 \frac{\partial p_0}{\partial y} && (15a)\\
T(\mathbf{u})_{12} &= \mu \left(\frac{\partial u_1}{\partial y} + \frac{\partial u_2}{\partial x} \right) && (15b)\\
T(\mathbf{u})_{21} &= \mu \left(\frac{\partial u_1}{\partial y} + \frac{\partial u_2}{\partial x} \right) && (15c)\\
T(\mathbf{u})_{22} &= (2\mu + \lambda)\frac{\partial u_2}{\partial y} + \lambda \frac{\partial u_1}{\partial x} + u_2 \frac{\partial p_0}{\partial y}, && (15d)
\end{aligned}
$$

and after some algebra, we find that

$$\frac{\partial \widetilde{u}_1}{\partial x} = \frac{\partial u_1}{\partial x} + \frac{1-2\nu}{2\mu(1-\nu)} u_2 \frac{\partial p_0}{\partial y} \tag{16a}$$

$$\frac{\partial \widetilde{u}_2}{\partial y} = \frac{\partial u_2}{\partial y} + \frac{1-2\nu}{2\mu(1-\nu)} u_2 \frac{\partial p_0}{\partial y} \tag{16b}$$

$$\frac{\partial \widetilde{u}_1}{\partial y} = \frac{\partial u_1}{\partial y} \tag{16c}$$

$$\frac{\partial \widetilde{u}_2}{\partial x} = \frac{\partial u_2}{\partial x}. \tag{16d}$$

From Equation (16), it follows that the approximation $\phi = I$ is valid in the limit $\nu = 0.5$ because the components of $\sigma(\widetilde{\mathbf{u}})_{ij}$ and $T(\mathbf{u})_{ij}$ coincide. But for incompressible solids, Equation (9) is ill-posed since the rheological relation between displacements, strain, and stress, in Equation (6) is undefined as λ goes to infinity. Hence, the approximation $\phi = I$ is not valid in this framework, and in the next section we address how to reformulate Equation (1) so that it becomes well-posed also in the purely incompressible limit.

4 Framework II: Mixed u-p-formulation

It is seen from the definition of the Lamé coefficient λ that when ν approaches 0.5, it goes to infinity. This makes the problem in Equation (5) ill-posed, and the corresponding stiffness matrix in Equation (7) becomes extremely ill-conditioned. This is the mathematical formulation of the phenomenon known as *volumetric locking*, which may lead to erroneous results when solving Equation (6) in the nearly incompressible limit. See, for example, [9], for further details on the locking effect.

A known remedy to the locking problem is to introduce the *scaled kinematic pressure* $p = \frac{\lambda}{\mu} \nabla \cdot \mathbf{u}$, and reformulate Equation (6) as a coupled system of PDEs, which yields

$$-\nabla \cdot (2\mu\varepsilon(\mathbf{u})) - \nabla(\mathbf{u} \cdot \nabla p_0) + (\nabla \cdot \mathbf{u})\nabla p_0 - \mu \nabla p = \mathbf{f} \text{ in } \Omega \tag{17a}$$

$$\mu \nabla \cdot \mathbf{u} - \frac{\mu^2}{\lambda} p = 0 \text{ in } \Omega \tag{17b}$$

$$[2\mu\varepsilon(\mathbf{u}) + \mu p I] \cdot \mathbf{n} = \ell \text{ on } \Gamma_L \tag{17c}$$

$$[2\mu\varepsilon(\mathbf{u}) + \mu p I] \cdot \mathbf{n} = \mathbf{0} \text{ on } \Gamma_N \tag{17d}$$

$$\mathbf{u} = \mathbf{0} \text{ on } \Gamma_D \tag{17e}$$

$$u_1 = 0, \partial_x u_2 = 0 \text{ on } \Gamma_S. \tag{17f}$$

In Equation (17), the GIA momentum balance equation is transformed into a form that is valid for all $\nu \in [0, 0.5]$. Such systems of PDEs are possible to handle in ABAQUS, but as is described in Section 3 it is not possible to model the first order terms in Equation (17a). Therefore, we have written our own FE software to solve this problem, where we include the advection and buoyancy terms and model the full non-self gravitating GIA problem.

4.1 Finite Element Discretization

In this subsection we consider the properties of the finite element problem corresponding to a generalized form of Equation (17), which reads,

$$\begin{array}{l}\text{Find } \mathbf{u} \in \mathbf{V} \subset \mathbf{H}^1 \text{ and } p \in P = \{p \in L^2 : \int_\Omega p = 0\} \text{ such that} \\ \begin{array}{rcll} a(\mathbf{u},\mathbf{v}) + b(\mathbf{v},p) & = & \mathbf{f}(\mathbf{v}) + \langle \ell, \mathbf{v}_h \rangle & \forall \mathbf{v} \in \mathbf{V}, \\ b(\mathbf{u},q) - c(p,q) & = & 0, & \forall q \in P. \end{array}\end{array} \tag{18}$$

The bilinear forms in Equation (18) read as follows

$$\begin{aligned} a(\mathbf{u},\mathbf{v}) &= \int_\Omega 2\mu\varepsilon(\mathbf{u}) : \varepsilon(\mathbf{v}) - \nabla(\mathbf{u}\cdot\mathbf{b})\cdot\mathbf{v} + (\nabla\cdot\mathbf{u})(\mathbf{c}\cdot\mathbf{v}) d\Omega \\ b(\mathbf{u},p) &= \int_\Omega \mu(\nabla\cdot\mathbf{u}) p \, d\Omega \qquad c(p,q) = \int_\Omega \frac{\mu^2}{\lambda} p\, q \, d\Omega \\ \langle \ell, \mathbf{v}\rangle &= \int_\Gamma \mathbf{v}\cdot\ell \, d\Gamma \qquad \mathbf{f}(\mathbf{v}) = \int_\Omega \mathbf{f}\cdot\mathbf{v}\, d\Omega, \end{aligned} \tag{19}$$

where $\mathbf{b}$ and $\mathbf{c}$ describe general vector fields. The boundary of the computational domain Ω is denoted by Γ.

The general theory for variational problems of type (18) postulates that to ensure existence and uniqueness for the solution of Equation (18), two groups of conditions must be satisfied.

First, $a(\mathbf{u},\mathbf{v})$, $c(p,q)$ and $b(\mathbf{v},p)$ have to be bounded, i.e., there exists constants $\overline{a}$, $\overline{b}$, $\overline{c}$, independent of $\mathbf{u}$, $\mathbf{v}$, p, q and the discretization parameter h, such that

$$a(\mathbf{u},\mathbf{v}) \leq \overline{a}\|\mathbf{u}\|_{\mathbf{V}}\|\mathbf{v}\|_{\mathbf{V}} \quad \forall \mathbf{u},\mathbf{v} \in \mathbf{V} \tag{20}$$

$$b(\mathbf{v},p) \leq \overline{b}\|\mathbf{v}\|_{\mathbf{V}}\|p\|_P \quad \forall \mathbf{u} \in \mathbf{V},\, p \in P \tag{21}$$

$$c(p,q) \leq \overline{c}\|p\|_P\|q\|_P \quad \forall p,q \in P. \tag{22}$$

The second condition is that $a(\mathbf{u},\mathbf{u})$ and $c(p,p)$ must be coercive on $\mathbf{V}$ and P, respectively. That is, if

$$a(\mathbf{u},\mathbf{u}) \geq \underline{a}\|\mathbf{u}\|^2_{\mathbf{V}}, \quad \underline{a} > 0 \quad \forall \mathbf{u} \in \mathbf{V} \tag{23}$$

$$c(p,p) \geq \underline{c}\|p\|^2_P, \quad \underline{c} > 0 \quad \forall p \in P. \tag{24}$$

As is clear from Equation (19), $c(p,q) = 0$, $\forall p,q \in P$ corresponds to $\nu = 0.5$. In this case, Equation (18) is solvable if (i) conditions (20) - (22) hold, (ii) if $a(\mathbf{u},\mathbf{u})$ is coercive on the null-space of $b(\mathbf{u},q)$, and (iii) if $b(\mathbf{u},q) = 0 \quad \Rightarrow q = 0 \quad \forall \mathbf{u} \in \mathbf{V}$.

Furthermore, Equation (18) is stable if the following inf-sup (or Ladyzhenskaya-Babuška-Brezzi or LBB) conditions are fulfilled,

$$\inf_{\mathbf{u}\in\mathbf{V}} \sup_{\mathbf{v}\in\mathbf{V}} \frac{a(\mathbf{u},\mathbf{v})}{\|\mathbf{u}\|_{\mathbf{V}}\|\mathbf{v}\|_{\mathbf{V}}} \geq \underline{a}' > 0, \tag{25}$$

and

$$\inf_{q\in P} \sup_{\mathbf{v}\in\mathbf{V}} \frac{b(\mathbf{u},q)}{\|\mathbf{v}\|_{\mathbf{V}}\|q\|_P} \geq \underline{b}' > 0, \tag{26}$$

for some constants $\underline{a}'$ and $\underline{b}'$ independent of $\mathbf{u}$, $\mathbf{v}$, p, q and the discretization parameter h. Note that when $a(\mathbf{u},\mathbf{v})$ is coercive, condition (25) is automatically satisfied. For details, see for example [10].

The coercivity of $c(p,q)$ is straightforwardly seen, the condition (26) is guaranteed by the theory for the Stokes problem [9], and in [7] it is shown

that the bilinear forms in Equation (18) are bounded. What remains to ensure the solvability of Equation (17) is the condition in Equation (25). In [7] it is shown that $a(\mathbf{u}, \mathbf{u})$ is in general not coercive due to the first order terms.

In [5], we study the case of a homogeneous, incompressible solid and for this particular case we derive sufficient boundary conditions on the anti-symmetric part of the displacement tensor $\nabla \mathbf{u}$ and the advection of the pre-stress that ensures the coercivity of $a(\mathbf{u}, \mathbf{u})$.

In this paper the coercivity of the bilinear form $a(\mathbf{u}, \mathbf{u})$ in its full complexity is not discussed, as we study materials that are described by the Models $C0$ and $C1$ only.

For the Model $C0$, the coercivity of $a(\mathbf{u}, \mathbf{u})$ is given by the Korn inequality,

$$a(\mathbf{u}, \mathbf{u}) = \int_\Omega 2\mu\varepsilon(\mathbf{u}) : \varepsilon(\mathbf{u})\, d\Omega \geq K(\Omega) \int_\Omega 2\mu \sum_{k=1}^{d} \nabla u_k \cdot \nabla u_k, \tag{27}$$

where $K(\Omega)$ is the *Korn constant*. This parameter is known to depend only on the computational domain and the boundary conditions, see for example [2]. Therefore, there exists a positive real number C, such that

$$a(\mathbf{u}, \mathbf{u}) \geq C\|\mathbf{u}\|_{\mathbf{V}}^2.$$

For the Model $C1$, the situation is more elaborate, and the material density (ρ_r) and the gravitational acceleration (g) cannot be chosen independently from C.

In [7] it is shown that the Gårding-type relation

$$a(\mathbf{u}, \mathbf{u}) \geq C^{(1)}\|\mathbf{u}\|_{\mathbf{V}}^2 - C^{(2)}\|\mathbf{u}\|_0^2 \tag{28}$$

holds, where $C^{(1)} = C - \eta\frac{\varepsilon}{2}$, $C^{(2)} = \frac{\eta}{2\varepsilon}$, and ε is an arbitrary, positive, real number. The parameter $\eta = d(\alpha_1 + \alpha_2 + \beta)$, where

$$|b_i(x)| \leq \alpha_1, \quad i = 1, \ldots, d, \tag{29}$$

$$|\nabla \cdot \mathbf{b}| \leq \alpha_2, \tag{30}$$

$$|c_i(x)| \leq \beta, \quad i = 1, \ldots, d. \tag{31}$$

For the Model $C1$, $\mathbf{b} = [0, -\rho_r g]^T$ and $\mathbf{c} = \mathbf{0}$, and hence, $\alpha_1 = \rho_r g$ and $\alpha_2 = \beta = 0$. From the relation $\|\cdot\|_{\mathbf{V}} = \|\cdot\|_1 \geq \|\cdot\|_0$, we have that

$$a(\mathbf{u}, \mathbf{u}) \geq \left(C - \frac{\varepsilon d\rho_r g}{2} - \frac{d\rho_r g}{2\varepsilon}\right)\|\mathbf{u}\|_{\mathbf{V}}^2. \tag{32}$$

From Equation (32), it follows that $a(\mathbf{u}, \mathbf{u})$ is coercive when

$$C - \frac{\varepsilon d\rho_r g}{2} - \frac{d\rho_r g}{2\varepsilon} > 0,$$

that is, for ε in the interval

$$\frac{C}{d\rho_r g}\left(1 - \sqrt{1 - \frac{(d\rho_r g)^2}{C^2}}\right) < \varepsilon < \frac{C}{d\rho_r g}\left(1 + \sqrt{1 - \frac{(d\rho_r g)^2}{C^2}}\right).$$

As ε is real and positive, it is required that

$$\frac{(d\rho_r g)^2}{C^2} < 1. \tag{33}$$

The last condition is of limited practical use because the constant C is not known in general. Therefore, what we can conclude from Equation (33) is that there exists combinations of problem geometry, boundary conditions, and material parameters, such that the solution to Equation (18) exists and is unique. Unfortunately, we cannot determine these combinations explicitely. However, when the numerical experiments that are accounted for in Section 5 are performed, there are no signs of unstable or erratic behavior in the obtained solutions. This indicates that for physically reasonable material parameters and boundary conditions, the bilinear form $a(\mathbf{u}, \mathbf{u})$ is actually coercive, and the solution to Equation (18) exist and is unique.

4.2 The Algebraic Problem

The algebraic problem corresponding to Equation (17) takes the form,

$$\mathcal{A}\mathbf{x} = \begin{bmatrix} M & B^T \\ B & -C \end{bmatrix} \begin{bmatrix} \mathbf{x}_1 \\ \mathbf{x}_2 \end{bmatrix} = \begin{bmatrix} \mathbf{b} \\ \mathbf{0} \end{bmatrix}, \tag{34}$$

where $M \in \mathbb{R}^{N_u \times N_u}$ is non-symmetric, sparse and in general indefinite, and $C^{N_p \times N_p}$ is positive semi-definite. The system matrix $\mathcal{A} \in \mathbb{R}^{N \times N}$, where $N = N_u + N_p$.

The algebraic problem in Equation (34) is solved with an iterative solution method preconditioned by the block-lower triangular matrix

$$\mathcal{D} = \begin{bmatrix} D_1 & 0 \\ B & -D_2 \end{bmatrix}, \tag{35}$$

where the first diagonal block D_1 approximates M, and the second diagonal block, D_2, approximates the negative Schur complement of $\mathcal{A}$, $S = C + BM^{-1}B^T$. The block-triangular matrix $\mathcal{D}$ is only one possible choice of a preconditioner for $\mathcal{A}$ and we refer to [8] for a recent and extensive survey over existing preconditioning and solution techniques for saddle point problems.

To actually form S is, unless for some special cases, about as expensive as it is to solve the system with $\mathcal{A}$, and the arising matrix is in general dense even if $\mathcal{A}$ is sparse. Good approximations for the Schur complement matrix are known in some cases, for example, for the Stokes problem one can replace $BM^{-1}B^T$ by the pressure mass matrix. We note, that in our case this would lead to a symmetric D_2, while the true S is nonsymmetric.

We use here a simple technique, based on the finite element framework, which enables us to compute a matrix D_2 which is (i) sparse, (ii) computed at low cost, and (iii) inherits the symmetricity or nonsymmetricity of $\mathcal{A}$. To this end, we note that the global stiffness matrix $\mathcal{A}$ is assembled from element stiffness matrices $\mathcal{A}_E$, which are of the same saddle point form as $\mathcal{A}$ itself, namely

$$\mathcal{A} = \sum_E \mathcal{A}_E \quad \text{where} \quad \mathcal{A}_E = \begin{bmatrix} M_E & B_E^T \\ B_E & -C_E \end{bmatrix}.$$

As long as M_E is non-singular [1], we can compute exactly the local Schur complement of each $\mathcal{A}_E$, $S_E = C_E + B_E M_E^{-1} B^T$, and assemble these local contributions to form D_2, $D_2 = \sum_E S_E$. See [7] for further details.

[1] The non-singularity of M_E can always be enforced by adding a regularization term to its diagonal, $\widetilde{M}_E = M_E + \epsilon h^2 I$, where $0 < \epsilon \ll 1$ and h is the discretization parameter.

To compute the action of $\mathcal{D}^{-1}$ on a vector, we have to solve systems with D_1 and D_2. We choose to do the latter by an efficient inner iterative solution method, equipped with a robust preconditioner for each of the blocks.

4.2.1 Preconditioners for D_1 and D_2

.

For D_1, the preconditioner is constructed in the following way. The entries of the block M are given by the bilinear form $a(\mathbf{u}, \mathbf{v})$, $m_{ij} = a(\mathbf{u}_i, \mathbf{v}_j)$, which is non-symmetric due to the presence of the pre-stress advection term. The advection term is, however, not dominating the problem, and therefore the matrix $\widehat{M}$, whose entries are given by the bilinear form

$$\widehat{M}_{i,j} = \widehat{a}(\mathbf{v}_i, \mathbf{v}_j) = \int_\Omega 2\mu\varepsilon(\mathbf{v}_i) : \varepsilon(\mathbf{v}_j)\, d\Omega,$$

could be expected to be a reasonably good preconditioner to M.

If we assume that the unknown displacements are ordered in the so-called 'separate displacement ordering', we know from the classical linear elasticity theory that, due to Korns inequality, the block-diagonal part of $\widehat{M}$ is a nearly optimal preconditioner to $\widehat{M}$, cf. [2].

Furthermore, it suffices to replace these diagonal blocks by a scaled vector-valued Laplacian matrix $\widetilde{M}$, corresponding to the bilinear form

$$\widetilde{M}_{i,j} = \widetilde{a}(\mathbf{v}_i, \mathbf{v}_j) = \int_\Omega \sum_{k=1}^{d} 2\mu\nabla u_{k,i} \cdot v_{k,j}\, d\Omega, \quad \mathbf{v}_i = [v_{1,i}, \ldots, v_{d,i}]^T, \quad (36)$$

that obeys the same boundary conditions as M.

Based on the latter result, the inner iterative solver for D_1 is preconditioned by a block-diagonal matrix $\widetilde{M}$, whos diagonal blocks consists of scaled Laplacian matrices. To each of these blocks, as well as to the matrix D_2, we apply a robust and efficient multilevel preconditioner. In [6] this approach is investigated and it is found there that the smallest overall solution time for the system with $\mathcal{A}$ is achieved when D_1 and D_2 are solved to a relative accuracy of 0.5.

To implement the above described preconditioner, we use a code developed by the first author. This code is based on the open source packages `deal.II` [4] and `PETSc` [16].

5 Numerical Experiments

The numerical experiments are performed on two problems, denoted *Uniform Load* and *Footing Problem*.

Problem 5.1 *(Uniform Load). A 2D (3D) flat Earth model is subjected to a uniform load from a 2.14 km thick ice sheet. The size of the domain is 10 000 km width (side) and 4000 km depth. The boundary conditions are homogeneous Dirichlet conditions on the boundary $y = -4000$ km ($z = -4000$ km) and symmetry conditions on the vertical boundaries $x = 0$ and $x = 10000$ (and $y = 0$ and $y = 10000$). The geometry of the problem in two space dimensions is shown in Figure 2.*

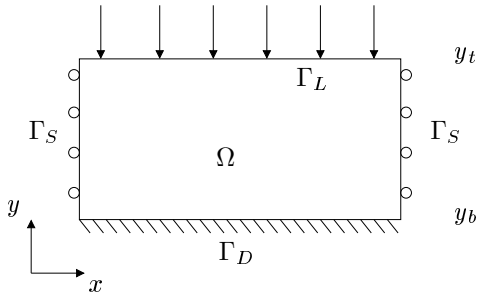

Figure 2: Problem 5.1, Uniform Load. The geometry of the problem.

Table 1: The material parameters used in Problem 5.1 and 5.2.

Parameter		Value
Rock density	ρ_r	3300 $kg\ m^{-3}$
Ice density	ρ_i	917 $kg\ m^{-3}$
Youngs modulus	E	400 GPa
Poisson ratio	ν	$[0.2, 0.4999999]$

Problem 5.2 *(Footing Problem). A 2D (3D) flat Earth model, which is symmetric with respect to $x = 0$ (and $y = 0$), is subjected to a Heaviside load of a 1000 km wide (side) and 2.14 km thick ice sheet. The size of the domain is 10 000 km width and 4000 km depth. The boundary conditions are as follows: homogeneous Dirichlet conditions on the boundary $y = -4000$ km ($z = -4000$ km) and symmetry conditions on the boundary $x = 0$ (and $y = 0$), homogeneous Neumann conditions on the boundary $x = 10000$ km (and $y = 10000$ km) and the boundary segment $y = 0$ ($z = 0$), $x > 1000$ km (and $y > 1000$ km). The geometry of this problem in two space dimensions is similar to the geometry shown in Figure 1.*

The material parameters for Problem 5.1 and 5.2 are given in Table 1.

The computational domain is discretized with uniform rectangular finite elements in 2D and brick finite elements in 3D. Standard bilinear basis functions are applied in Framework I (ABAQUS), whereas in Framework II, a stable pair of finite element basis functions for $\mathbf{u}$ and p is used, namely, the modified Taylor–Hood ($Q1$ -iso $Q1$) discretization. That is, the basis functions for the displacements $\mathbf{u}$ live on a mesh that is a uniform refinement of the mesh on which the pressure variables p live. The meshes are chosen in such a way that the number of displacement degrees of freedom are the same for both Framework I and Framework II. This makes the linear system to solve in Framework II larger than that in Framework I, roughly 13 % for $d = 2$ and 8 % for $d = 3$.

In Framework I, the algebraic problem $\mathcal{A}\mathbf{x} = \mathbf{b}$ is solved with a direct method, provided by ABAQUS, whereas in Framework II, the generalized conjugate gradient - minimal residual method (GCG-MR, cf. [3]) is chosen as an iterative solver both for the outer iterative solver for $\mathcal{A}$, and for the two inner iterative solvers for D_1 and D_2. The outer iterative solver is stopped when the initial residual is reduced by six orders of magnitude.

Unless stated otherwise, the absolute errors reported in this section are measured in $\|\cdot\|_N$-norm, that is, for two arbitrary vectors $\mathbf{u}, \mathbf{v} \in \mathbb{R}^N$,

the error is given by

$$\|\mathbf{u}-\mathbf{v}\|_N = \frac{1}{N}\sqrt{\sum_{i=1}^{N}(u_i - v_i)^2}.$$

The relative errors are measured in the discrete ℓ^2-norm,

$$e(\mathbf{u},\mathbf{v}) = \frac{\|\mathbf{u}-\mathbf{v}\|_{\ell^2}}{\|\mathbf{u}\|_\ell^2}.$$

Throughout this Section, if not stated otherwise, $\mathbf{u}_I$ and $\mathbf{u}_{II}$ denote the numerical solutions obtained from Framework I and II, respectively. The solution $\mathbf{u}$ is the exact (analytical) solution to Problem 5.1 (the Uniform Load problem).

5.1 Results for Problem 5.1

5.1.1 Analytical Results

For a $C1$ solid, the two-dimensional version of Problem 5.1 is described by the BVP

$$-\nabla\cdot\sigma - \nabla(\mathbf{u}\cdot\nabla p_0) = 0 \qquad \text{in } \Omega \tag{37a}$$
$$\sigma\cdot n = \ell \qquad \text{on } \Gamma_L \tag{37b}$$
$$\mathbf{u} = 0 \qquad \text{on } \Gamma_D \tag{37c}$$
$$u_1 = 0, \quad \frac{\partial u_2}{\partial x} = 0 \qquad \text{on } \Gamma_S, \tag{37d}$$
$$\tag{37e}$$

with $\ell = [0, -\rho_i g h_i]$ and $\nabla p_0 = -\rho_r g\hat{\mathbf{y}}$. Equation (37) has an analytical solution

$$\begin{aligned} u_1 &= 0 \\ u_2 &= \frac{\rho_i h_i}{\rho_r}\left(e^{\frac{-\rho_r g(y_t-y_b)}{2\mu+\lambda}} - e^{\frac{-\rho_r g(y_t-y)}{2\mu+\lambda}}\right), \end{aligned} \tag{38}$$

whereas, for a solid described by the $C0$ model, the analytical solutions reads

$$\begin{aligned} u_1 &= 0 \\ u_2 &= -\frac{\rho_i g h_i (y-y_b)}{2\mu+\lambda}. \end{aligned} \tag{39}$$

When Equation (37) is reformulated in Framework I, by introducing the modified stress tensor $T(\mathbf{u})$, the exact solution to the so-arising BVP is then

$$\begin{aligned} \widetilde{u}_1 &= 0 \\ \widetilde{u}_2 &= -\frac{\rho_i g h_i (y-y_b)}{(2\mu+\lambda)+\rho_r g(y_t-y_b)}. \end{aligned} \tag{40}$$

The first two terms in the Taylor expansion of u_2 in Equation (38) read,

$$u_2 \approx -\frac{\rho_i g h_i (y-y_b)}{2\mu+\lambda} - \frac{\rho_i\rho_r g^2 h_i}{(2\mu+\lambda)^2}\frac{(y-y_b)(2y_t-y_b-y)}{2}, \tag{41}$$

Table 2: Problem 5.1, Uniform Load. The norm of E_2 for different values of the Poisson's ration.

ν	$\|E_2\|_N$
0.2	0.11161
0.3	0.076035
0.4	0.030007
0.45	0.0095767
0.47	0.0038158
0.49	0.00047043
0.4999	4.9577e-08
0.49999	4.96e-10
0.499999	4.9603e-12
0.4999999	4.9603e-14

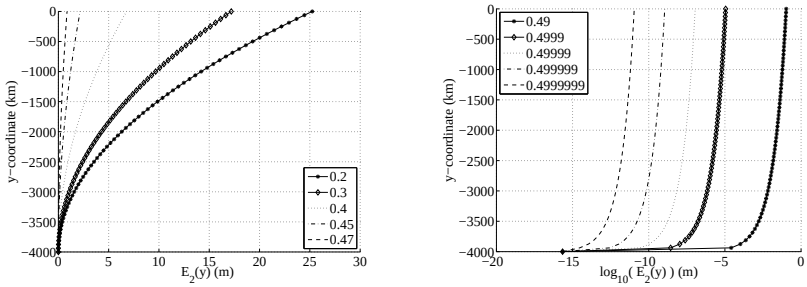

(a) $\nu = 0.2, \ldots, 0.47$ (b) $\nu = 0.49, \ldots, 0.4999999$

Figure 3: Problem 5.1, Uniform Load. E_2, the leading term in $u_2 - \widetilde{u}_2$ as of function of depth for values of the Poisson ratio ranging form 0.2 to 0.4999999. The scale on the horizontal axis in figure (b) is logarithmic.

and assuming that

$$\left| \frac{\rho_r g(y_t - y_b)}{2\mu + \lambda} \right| < 1,$$

the two leading terms in the expansion of $\widetilde{u}_2$ become

$$\widetilde{u}_2 \approx -\frac{\rho_i g h_i (y - y_b)}{2\mu + \lambda} - \frac{\rho_i \rho_r g^2 h_i}{(2\mu + \lambda)^2}(y - y_b)(y_t - y_b). \tag{42}$$

Hence, the error in the solution to Equation (37) produced in Framework I is of the order of the difference between Equation (41) and Equation (42), that is

$$u_2 - \widetilde{u}_2 = \mathcal{O}\left(E_2(y)\right), \text{ where } E_2(y) = \frac{\rho_i \rho_r g^2 h_i (y - y_b)^2}{2(2\mu + \lambda)^2}. \tag{43}$$

The behavior of E_2 for different values of the Poisson's ratio is illustrated in Table 2 and Figure 3. In the table the norm of $\mathbf{E}_2$, $\|\mathbf{E}_2\|_N$ is shown, where $\mathbf{E}_2$ is a vector containing values of E_2 sampled at different depths. That is, $(\mathbf{E}_2)_k = E_2(y_k)$, where $k = 1, \ldots, N$, and $y_1 = y_b$ and $y_N = y_t$. Figure 3, $E_2(y)$ for different ν is plotted as a function of the depth.

Table 3: Problem 5.1, Uniform Load. The absolute error $\|\mathbf{u}_j - \mathbf{u}\|_N$, $j = I, II$ in the numerical solution. The number d denotes the number of space dimensions, and the problem size $N = 23603$ for $d = 2$ and $N = 12512$ for $d = 3$.

	Framework I		Framework II	
$d = 2$				
ν	Model $C0$	Model $C1$	Model $C0$	Model $C1$
0.2	1.8517e-06	0.065342	8.5363e-07	2.2743e-06
0.3	1.5971e-06	0.048653	1.1354e-06	1.746e-06
0.4	2.6633e-07	0.022546	1.7717e-06	4.4683e-06
0.45	2.5045e-07	0.0081289	2.7232e-07	1.2333e-06
0.47	2.3427e-07	0.0034382	6.2413e-08	1.5651e-06
0.49	9.8936e-08	0.0004534	3.0402e-07	3.1054e-07
0.4999	2.8362e-09	4.9419e-08	4.9874e-07	1.8228e-07
0.49999	2.799e-09	2.8278e-09	4.9718e-07	1.8103e-07
0.499999	2.8765e-09	2.877e-09	4.9703e-07	1.8091e-07
0.4999999	2.8283e-09	2.8283e-09	4.9702e-07	1.809e-07
$d = 3$				
ν	Model $C0$	Model $C1$	Model $C0$	Model $C1$
0.2	2.6177e-06	0.11709	2.3552e-07	0.00016957
0.3	3.2162e-06	0.086805	7.5379e-07	0.00024097
0.4	4.4583e-07	0.039929	5.0682e-07	0.00017129
0.45	3.919e-07	0.014322	5.6226e-07	7.1704e-05
0.47	3.6656e-07	0.006043	1.0061e-06	3.1838e-05
0.49	8.7572e-08	0.00079496	5.4925e-07	4.9122e-06
0.4999	2.5154e-09	8.8134e-08	6.7687e-07	5.3945e-07
0.49999	1.7387e-10	9.4708e-10	6.7911e-07	5.4061e-07
0.499999	1.97e-11	2.9118e-11	6.7934e-07	5.4074e-07
0.4999999	1.7169e-12	1.6935e-12	6.7936e-07	5.4075e-07

Remark 5.1 *Equations* (37) - (43) *are expressed in two space dimensions only, but the results can be directly carried over to the three dimensional case.*

5.1.2 Experimental Results

Table 3 shows the absolute errors for $\mathbf{u}_I$ and $\mathbf{u}_{II}$ compared to the exact solution of Equation (38) (Model $C1$) and Equation (39) (Model $C0$). For Model $C0$, both $\mathbf{u}_I$ and $\mathbf{u}_{II}$ coincide with the exact solution. For Model $C1$, the error in $\mathbf{u}_I$ is of the same order of magnitude as E_2, and it can be noticed that the agreement between $\|\mathbf{u}_I - \mathbf{u}\|_N$ and $\|E_2\|_N$ in Table 2 is better for $d = 3$ than for $d = 2$. The solution from Framework II, $\mathbf{u}_{II}$, coincides with the exact solution up to the convergence criterion of the iterative solver (six orders of magnitude). To get an idea about the absolute difference between the solution to Equation (38) (Model $C1$) obtained from Framework I and II, Table 4 show the vertical component of $\mathbf{u}_I$ and $\mathbf{u}_{II}$ at the surface $y = y_t$ for $\nu = 0.2$ and $\nu = 0.4999$. The horizontal component is zero.

In Table 5 timings for the stiffness matrix assembly phase and the

Table 4: Problem 5.1, Uniform Load. The vertical displacement u_2 on the surface $y = y_t$.

	Framework I	Framework II
$\nu = 0.2$	-134.142	-150.272
$\nu = 0.4999$	-0.11543	-0.11546

Table 5: Problem 5.1, Uniform Load. Timings for the assembly phase and the solution phase for the two frameworks for the Model $C1$ and Poisson ratio $\nu = 0.3$. For Framework II, the figures in parentheses in the middle column under solution time are the time spent by the iterative solver, and the numbers in the rightmost column are the number of outer iterations, and average number of inner iterations for D_1 and D_2 per outer iteration, required. The number d denotes the number of space dimensions and N is the size of the system matrix in Framework II.

	Assembly time		Solution time		
$d = 2$					
N	Framework I	Framework II	Framework I	Framework II	
6043	0.8945	0.21777	1.0830	1.0195 (0.48633)	13 (1,1)
23603	2.9941	0.88574	4.2197	4.2246 (1.9951)	12 (1,1)
93283	11.882	3.9775	17.382	19.3838 (9.8135)	11 (2,1)
370883	51.438	17.7109	73.173	89.3389 (49.4287)	11 (2,1)
1479043	252.68	77.7022	309.99	431.769 (257.574)	12 (2,1)
$d = 3$					
N	Framework I	Framework II	Framework I	Framework II	
12512	1.5254	1.8994	3.0488	8.0088 (3.4649)	12 (2,1)
89700	14.088	8.7559	43.291	63.335 (33.0762)	13 (2,1)
678116	110.28	65.8047	1347.4	749.296 (506.795)	15 (4,1)

Table 6: $C0$ formulation of Problem 5.2, the Footing Problem. The table shows absolute and relative differences between $\mathbf{u}_I$ and $\mathbf{u}_{II}$ for different problem size and Poisson ration. The number d denotes the number of space dimensions and N is the size of the system matrix in Framework II.

	$\nu = 0.2$		$\nu = 0.4999999$	
$d = 2$				
N	$\|\mathbf{u}_I - \mathbf{u}_{II}\|_N$	$e(\mathbf{u}_I, \mathbf{u}_{II})$	$\|\mathbf{u}_I - \mathbf{u}_{II}\|_N$	$e(\mathbf{u}_I, \mathbf{u}_{II})$
6043	0.00044317	0.0010921	0.00085183	0.00248
23603	0.00038565	0.00095014	0.00056619	0.001648
93283	1.8287e-05	4.5052e-05	6.9302e-05	0.00020169
370883	5.0107e-06	1.2344e-05	3.0619e-05	8.9108e-05
1479043	1.6802e-06	4.1392e-06	1.5139e-05	4.4057e-05
$d = 3$				
N	$\|\mathbf{u}_I - \mathbf{u}_{II}\|_N$	$e(\mathbf{u}_I, \mathbf{u}_{II})$	$\|\mathbf{u}_I - \mathbf{u}_{II}\|_N$	$e(\mathbf{u}_I, \mathbf{u}_{II})$
12512	0.0012399	0.015093	0.003522	0.050982
89700	0.00041476	0.0050259	0.0014047	0.020366
678116	6.3e-05	0.00076169	0.00038702	0.0056037

solution phase for Framework I and II are shown. The solution phase in Framework I includes the factorization of the stiffness matrix and a direct solve with the two factors, while the solution phase in Framework II includes the assembly of the Schur complement approximation, the construction of the multilevel preconditioners for D_1 and D_2, and finally the time spent for the iterative solver. In Table 5 the latter time is reported within parentheses in the middle column under "Solution time". The rightmost column in the table shows the number of outer iterations, and the average number of inner iterations for $D1$ and $D2$ (in parentheses), required for convergence. Except for the two smallest problem sizes for $d = 3$, the overall time (assembly + solution) is lower for the solver in Framework II, than for that in Framework I, despite the fact that the problem size in Framework II is larger than the problem size in Framework I. The problem size N in this section refers to the size of the linear system obtained in Framework II.

5.2 Results for Problem 5.2

Tables 6 and 7 show absolute and relative differences between the solutions $\mathbf{u}_I$ and $\mathbf{u}_{II}$ to Problem 5.2 in two and three space dimensions for different problem sizes and Poisson ratios.

In Table 6 data for the $C0$-formulation of Problem 5.2, i.e. with prestress advection and buoyancy omitted, are shown. For both compressible ($\nu = 0.2$) and nearly incompressible ($\nu = 0.4999999$) solids, $\mathbf{u}_I$ and $\mathbf{u}_{II}$ seem to converge to the same solution in both two and three space dimensions. The difference between the two solutions are smaller for $d = 2$ than for $d = 3$ because the problem is better resolved in the first case.

Table 7 shows the errors between $\mathbf{u}_I$ and $\mathbf{u}_{II}$ for the $C1$-formulation of Problem 5.2. The differences between the solutions are larger for the

Table 7: $C1$ formulation of Problem 5.2, the Footing Problem. The table shows absolute and relative differences between $\mathbf{u}_I$ and $\mathbf{u}_{II}$ for different problem size and Poisson ration. The number d denotes the number space dimensions and N is the size of the system matrix in Framework II.

	$\nu = 0.2$		$\nu = 0.4999999$	
$d = 2$				
N	$\|\mathbf{u}_I - \mathbf{u}_{II}\|_N$	$e(\mathbf{u}_I, \mathbf{u}_{II})$	$\|\mathbf{u}_I - \mathbf{u}_{II}\|_N$	$e(\mathbf{u}_I, \mathbf{u}_{II})$
6043	0.046585	0.13214	0.0096158	0.030575
23603	0.046681	0.13238	0.0098538	0.031322
93283	0.046664	0.13233	0.0098168	0.0312
370883	0.046666	0.13233	0.0098362	0.03126
1479043	0.046666	0.13233	0.0098458	0.031289
$d = 3$				
N	$\|\mathbf{u}_I - \mathbf{u}_{II}\|_N$	$e(\mathbf{u}_I, \mathbf{u}_{II})$	$\|\mathbf{u}_I - \mathbf{u}_{II}\|_N$	$e(\mathbf{u}_I, \mathbf{u}_{II})$
12512	0.0073967	0.10003	0.0035596	0.057417
89700	0.0076817	0.10349	0.0016298	0.026383
678116	0.0077782	0.10455	0.00093842	0.015174

compressible solid than for the incompressible solid. This is in agreement with Equation (16) which says that the error in the modified stress tensor $\sigma(\widetilde{\mathbf{u}})$ compared to $T(\mathbf{u})$ vanishes in the incompressible limit. The absolute error for $d = 3$ is smaller than the absolute error for $d = 2$ simply because the displacements are smaller in the first case. This is due to the fact that for $d = 3$, the load is applied on 1 % of the upper surface, while for $d = 2$ the corresponding number is 10 %.

For $d = 3$ and $\nu = 0.4999999$, the difference between $\mathbf{u}_I$ and $\mathbf{u}_{II}$ decreases with growing problem size in a way that is not seen for $d = 2$. This is probably due to that the problem is better resolved in the latter case. For the two cases $d = 2$ and $N = 6043$, and $d = 3$ and $N = 678116$, the element size is the same (125 km). If we could solve larger problems for $d = 3$, we would probably have the same stabilization of the error as we have for $d = 2$.

To get an idea of how large the difference between $\mathbf{u}_I$ and $\mathbf{u}_{II}$ is, Figure 4 shows the horizontal and vertical displacements retrieved from Framework I and II on the surface $y = y_t$ for $\nu = 0.2$ and $\nu = 0.4999$.

Based only on the results in Table 7 it is impossible to decide which of $\mathbf{u}_I$ and $\mathbf{u}_{II}$ is the more accurate solution, but the data in Table 3 advocates that it should be $\mathbf{u}_{II}$.

6 Conclusions

In this paper, we report results from two different frameworks to model and numerically simulate the purely elastic response of the Earth to glaciation and deglaciation. The two frameworks differ in their ability to model the response for purely incompressible solids, in how the pre-stress advection is included, and in the way the algebraic problem that arises after a

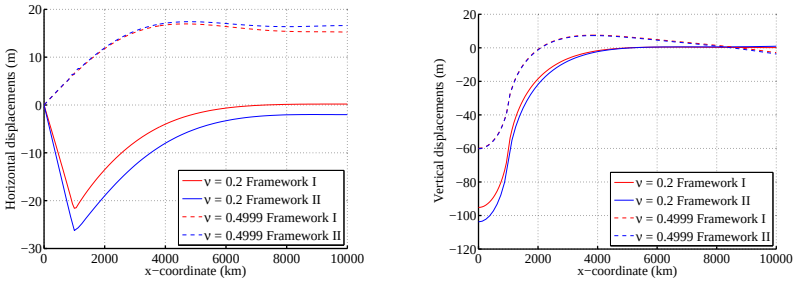

(a) $u_1|_{y=y_t}$ (b) $u_2|_{y=y_t}$

Figure 4: Problem 5.2, Footing Problem. The horizontal and vertical displacements on the surface $y = y_t$.

finite element discretization is solved.

Framework I is confined to the features of the general finite element package ABAQUS, which impose certain limitations on how to treat the pre-stress advection and the buoyancy terms. Framework II, while kept quite general, includes features to better model the underlying problem and provides a solution method which is both robust with respect to the full range of the problem parameters and highly numerically efficient. We find that Framework II gives a more accurate solution, and that this solution is achieved more efficiently compared to Framework I.

The higher efficiency in Framework II is achieved by using an efficient iterative solution method, preconditioned by a robust preconditioner instead of the direct solver in ABAQUS. Numerical experiments reveal that the preconditioned iterative solver is (i) a competitive alternative to the direct solver, (ii) nearly optimal, and (iii) scales almost linearly with the problem size in both two and three space dimensions.

The better accuracy obtained in Framework II is due to the fact that in this framework we discretize the momentum equations for GIA in their full complexity. This is not possible in Framework I due to the modeling constraints that are imposed by ABAQUS.

Acknowledgements

A first draft of this paper was written during the visit of the first author at the Institute of Parallel Processing, The Bulgarian Academy of Sciences, Sofia, in March and April 2006. He gratefully acknowledges the support obtained via EC INCO Grant BIS-21++ 016639/2005 which made this visit possible. Further, the authors are indebted to Dr Maya Neytcheva for giving insightful comments throughout the work on this paper and for proof-reading the manuscript.

The computations were carried out on a computer generously supplied by the Swedish Nuclear Fuel and Waste Management Co. (SKB).

References

[1] ABAQUS *ABAQUS manuals, version 6.5.* ABAQUS, Inc., 2004. http://www.abaqus.com [23 November 2006].

[2] Axelsson O. On iterative solvers in structural mechanics; separate displacement orderings and mixed variable methods. *Mathematics and Computers in Simulation*, 1999:**50**:11-30.

[3] Axelsson O. *Iterative solution methods*. Cambridge University Press, 1996.

[4] Bangerth W, Hartmann R, Kanschat G. `deal.II` Differential Equations Analysis Library, Technical Reference. IWR. http://www.dealii.org [27 October 2006].

[5] Bängtsson E, Lund B. A comparison between two approaches to solve the equations of linear isostasy. Technical Report 2006-03, Bulgarian IST Centre of Competence in 21 Century, 2006.

[6] Bängtsson E, Neytcheva M. An agglomerate multilevel preconditioner for linear isostasy saddle point problems. *Lecture Notes in Computer Science, Proceedings of the 5th International Conference on Large-scale Scientific Computations 2005*, Lirkov I, Margenov S, Wasniewski J (eds). 2006;**3743**:113-120.

[7] Bängtsson E, Neytcheva M. Numerical simulations of glacial rebound using preconditioned iterative solution methods. *Applications of Mathematics* 2005;**50**(3):183-201.

[8] Benzi M, Golub GH, Liesen J. Numerical solution of saddle point problems. *Acta Mathematica*, 2005:1-137.

[9] Braess D. *Finite elements. Theory, fast solvers, and applications in solid mechanics*. Cambridge University Press (2nd edn), 2001.

[10] Brezzi F, Bathe KJ. A discourse on the stability conditions for mixed finite element formulations. *Computer Methods in Applied Mechanics and Engineering* 1990;**82**:27-57.

[11] Han D, Wahr J. The viscoelastic relaxation of a realistically stratified earth, and a further analysis of postglacial rebound. *Geophysics Journal International* 1995;**120**:287-311.

[12] Johnston P. The effect of spatially non-uniform water loads on predictions of sea-level change. *Geophysics Journal International* 1993;**114**:615-634.

[13] Klemann V, Wu P, Wolf D. Compressible viscoelasticity: stability of solutions for homogeneous plane earth models. *Geophysics Journal International* 2003;**153**:569-585.

[14] Latychev L, Mitrovica JX, Tromp J, Tamisiea ME, Komatitsch D, Christara CC. Glacial isostatic adjustment on 3-d earth models: a finite volume formulation. *Geophysics Journal International* 2005;**161**:421-444.

[15] Martinec Z. Spectral-finite element approach to three-dimensional viscoelastic relaxation in a spherical earth. *Geophysics Journal International* 2000;**142**:117-141.

[16] Mathematics and Computer Science Division, Argonne National Laboratory. *Portable, Extensible Toolkit for Scientific computation (PETSc) suite*. http://www-unix.mcs.anl.gov/petsc/petsc-2/ [27 Oct 2006].

[17] Milne GA, Mitrovica JX. Postglacial sea-level change on a rotating earth. *Geophysics Journal International* 1998; **133**:1-19.

[18] Mitrovica JX, Milne GA, Davis JL. Glacial isostatic adjustment on a rotating earth. *Geophysics Journal International* 2001;**147**:562-578.

[19] Peltier WR. The impulse response of a maxwell earth. *Rev. Geophys. Space Phys.* 1974;**12**:649-669.

[20] Wolf D. Viscoelastodynamics of a stratified, compressible planet: incremental field equations and short- and long-time asymptotes. *Geophysics Journal International* 1991;**104**:401-417.

[21] Wu P. Using commercial finite element packages for the study of earth deformations, sea levels and the state of stress. *Geophysics Journal International* 2004:**158**:401-408.

[22] Wu P, Peltier WR. Viscous gravitational relaxation. *Geophys. J. R. Astro. Soc.*, 1982;**70**:435-485.

[23] Wu P, van der Wal W. Postglacial sealevels on a spherical, self-gravitating viscoelastic earth: effects of lateral viscosity variations in the upper mantle on the inference of viscosity contrasts in the lower mantle. *Earth and Planetary Science Letters* 2003;**211**:57-68.